High Runx1 Levels Promote a Reversible, More-Differentiated Cell State in Hair-Follicle Stem Cells during Quiescence

Lee, Song Eun
Department of Molecular Biology and Genetics, Cornell University

Sada, Aiko
Department of Molecular Biology and Genetics, Cornell University

Zhang, Meng
Department of Molecular Biology and Genetics, Cornell University

McDermitt, David J.
Department of Molecular Biology and Genetics, Cornell University

他

出版情報：Cell Reports. 6 (3), pp.499-513, 2014-02-13. Elsevier
バージョン：

Cell Reports
Article

Cell PRESS
Open ACCESS

High Runx1 Levels Promote a Reversible, More-Differentiated Cell State in Hair-Follicle Stem Cells during Quiescence

Song Eun Lee,[1] Aiko Sada,[1] Meng Zhang,[1] David J. McDermitt,[1] Shu Yang Lu,[1] Kenneth J. Kemphues,[1] and Tudorita Tumbar[1,*]
[1]Department of Molecular Biology and Genetics, Cornell University, Ithaca, NY 14853, USA
*Correspondence: tt252@cornell.edu
http://dx.doi.org/10.1016/j.celrep.2013.12.039

SUMMARY

Quiescent hair follicle (HF) bulge stem cells (SCs) differentiate to early progenitor (EP) hair germ (HG) cells, which divide to produce transit-amplifying matrix cells. EPs can revert to SCs upon injury, but whether this dedifferentiation occurs in normal HF homeostasis (hair cycle) and the mechanisms regulating both differentiation and dedifferentiation are unclear. Here, we use lineage tracing, gain of function, transcriptional profiling, and functional assays to examine the role of observed endogenous Runx1 level changes in the hair cycle. We find that forced Runx1 expression induces hair degeneration (catagen) and simultaneously promotes changes in the quiescent bulge SC transcriptome toward a cell state resembling the EP HG fate. This cell-state transition is functionally reversible. We propose that SC differentiation and dedifferentiation are likely to occur during normal HF degeneration and niche restructuring in response to changes in endogenous Runx1 levels associated with SC location with respect to the niche.

INTRODUCTION

Mammalian development and adult homeostasis are generally modeled as irreversible transitions between different cell states (Waddington, 1957). Dedifferentiation can be achieved by nuclear transfer or forced expression of master transcription factors (Pournasr et al., 2011). Germline transit-amplifying (TA) cells revert to stem cells (SCs) in the adult mouse and fly testis (Simons and Clevers, 2011; Spradling et al., 2011). In mammals, somatic TA cells, and sometimes even terminally differentiated lineages (TDL), can dedifferentiate to SCs in injury or cancer (Porrello et al., 2011; Schwitalla et al., 2013; Yanger et al., 2013). However, within normal uninjured somatic mammalian tissues, it is unclear to what extent distinct molecular and functional cell states may be reversible.

The adult hair follicle (HF) is composed largely of epithelial cells that form: (1) a permanent region (bulge) housing the HF SCs; (2) the temporary region (bulb) containing TA cells (matrix) and the TDL (inner root sheath [IRS] and hair core/shaft; Blanpain, 2010). The outermost root sheath (ORS) is contiguous with the bulge SC layer. The dermal papilla (DP) is a mesenchymal signaling center at the base of the bulb important for SC activation. HFs undergo cyclic phases of morphological remodeling known as the hair cycle (Blanpain, 2010). The hair-cycle phases are growth (anagen) when the bulge generates a new bulb, regression (catagen) when bulb cells die by apoptosis, and rest (telogen) when the bulge is quiescent (Müller-Röver et al., 2001).

In telogen, the bulb is replaced by the HG, which arises from quiescent bulge cells (Ito et al., 2004; Zhang et al., 2009). The HG fate is distinct from matrix and bulge fates, as shown by gene expression (Greco et al., 2009). Moreover, HG cells proliferate rapidly and then are lost from the dish (Greco et al., 2009), and at least the late-stage HG cells arising directly from bulge cells that migrate at telogen do not self-renew (Zhang et al., 2009). Thus, the HG acts as an "early progenitor" (EP), defined here as the first step of a bulge SC embarked on the path of differentiation toward a TA matrix cell. Bulge SCs self-renew at anagen by rare, symmetric divisions with respect to the basement membrane (Zhang et al., 2009, 2010).

Some of the ORS cells that migrated from the bulge at late anagen/early catagen remain below the bulge to eventually make a "new" HG and some move up to form a "new" bulge (Hsu et al., 2011). Importantly, it is not known whether the bulge SCs displaced into the ORS simply change location or actually differentiate into HG cells and then dedifferentiate upon returning to the new bulge. It is known that, in response to injury, such as hair plucking or LASER ablation, hair germ (HG) cells can dedifferentiate to bulge SCs (Ito et al., 2004; Rompolas et al., 2013). Whether this plasticity of fate is employed during normal hair homeostasis, the significance of a putative flexibility in cell fate in the absence of injury and a potential molecular mechanism remain a mystery.

Previously we showed that Runx1, a transcription factor from the Runt family (Blyth et al., 2005) is highly expressed in HG cells and is essential for their activation/proliferation and subsequent anagen onset (Hoi et al., 2010; Lee et al., 2013; Osorio et al.,

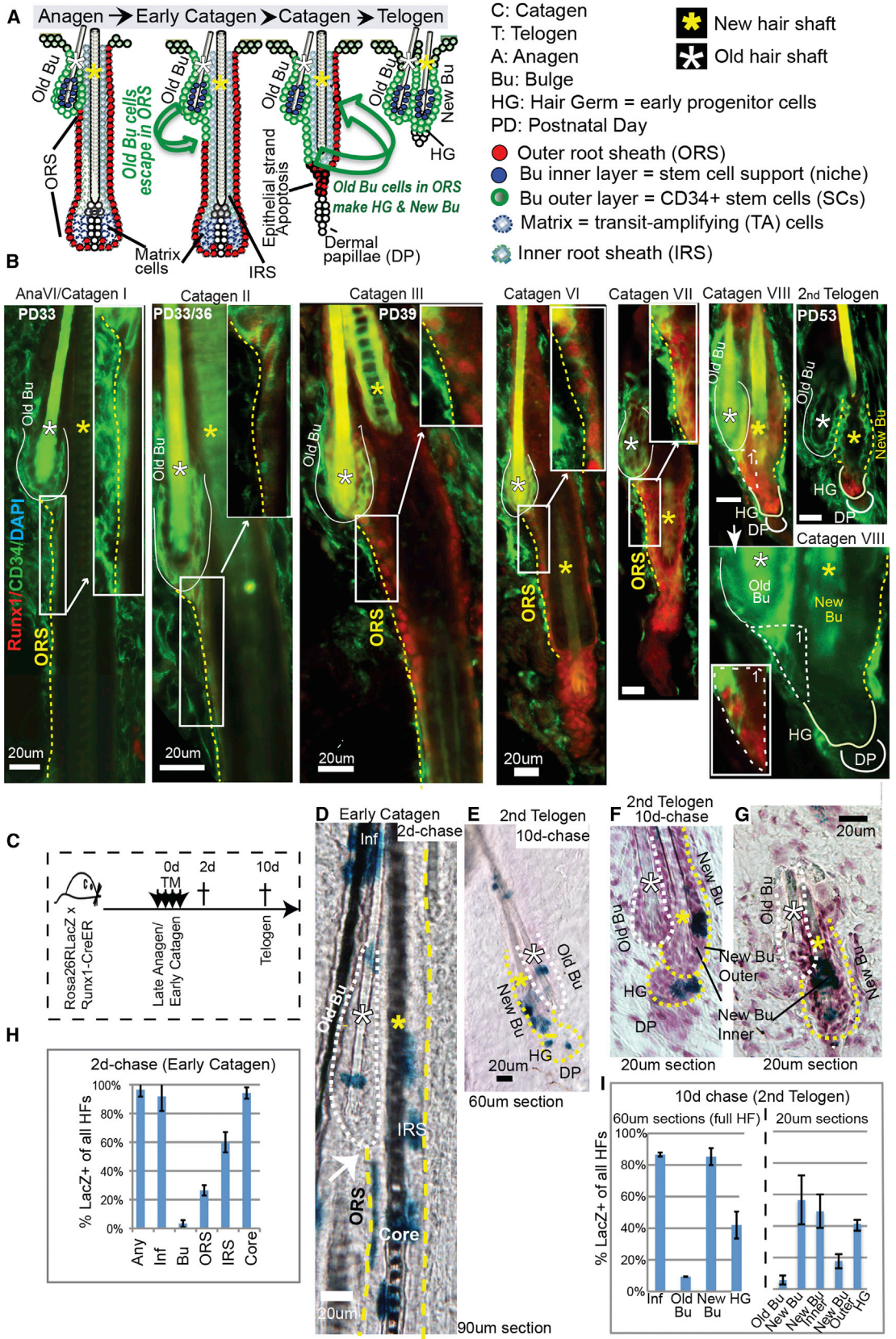

(legend on next page)

2008; Scheitz et al., 2012). Runx1 is even more highly expressed in the epithelial strand at late catagen (Osorio et al., 2008), suggesting a possible role at this stage of the hair cycle.

Here, we provide experimental evidence suggesting that increase in endogenous Runx1 levels during normal catagen has a dual function: (1) to induce degeneration of TA and TDL lineages and execute catagen, and (2) to promote a reversible differentiation of bulge SCs to HG EPs in the bulge cells that migrate into the ORS (Figure 1A; Hsu et al., 2011). This reversibility may ensure a proper balance between SC and EP populations during niche restructuring in normal tissue homeostasis.

RESULTS

ORS Cells that Once Expressed Runx1 Contribute to Both "New" Bulge and Hair-Germ Formation

Skin sections stained for endogenous Runx1 and CD34 (a bulge SC marker) showed that Runx1 became detectable in CD34$^+$ ORS cells just below the bulge by catagen II (Figure 1B). Based on location and CD34 expression, this ORS region must contain the migrated "old" bulge cells previously traced via H2B-GFP and Lgr5-CreER (Hsu et al., 2011). CD34 levels were generally higher in the old bulge than the ORS just below the bulge, whereas Runx1 showed the opposite trend (Figure 1B). At catagen VIII, the forming new bulge initially showed high Runx1/low CD34 levels but switched to low Runx1/high CD34 by the second telogen. These data suggest that quiescent bulge cells that have migrated into the ORS upregulate Runx1 at early catagen. By the second telogen, if they become "new" bulge cells, they downregulate Runx1, and if they become HG, they keep Runx1.

To test this, we marked Runx1$^+$ ORS cells at early second catagen and traced their lineage. Runx1-CreER;Rosa26RLacZ adult mice were injected with tamoxifen (TM) for 4 days starting at the sixth day after their skin turned from pink to black, indicative of anagen (~PD32; Figure 1C). We used thick, frozen skin sections that encompass full HFs (90 μm for catagen and 60 μm for telogen; Figures 1C–1I). We scored the compartments of each HF as positive or negative for LacZ$^+$ cells, irrespective of the total number of LacZ$^+$ cells in the compartment, to rule out proliferation effects.

Two days after the last TM injection (catagen; 2-day chase), we quantified the initial labeling of Runx1-expressing cells and found LacZ$^+$ cells in >95% of HFs, in a pattern expected from endogenous Runx1 expression (Figures 1D and 1H). In this stage, endogenous Runx1 is expressed weakly in the bulge, stronger in the ORS, and strongest in bulb cells including the differentiated lineages (Figures 1B and S1A) and also in the infundibulum (Inf) cells (Scheitz et al., 2012). About 60% of HFs showed LacZ$^+$ cells in the IRS (a terminally differentiated lineage −TDL), and >90% of HFs showed LacZ$^+$ cells in the hair shaft/core (another TDL) and Inf (Figure 1D). None of these lineages are expected to contribute normally to bulge SCs (Blanpain, 2010; Jaks et al., 2010) and HG regeneration (Greco et al., 2009; Hsu et al., 2011).

The lineages expected to contribute to the "new" bulge and HG are the "old" bulge and ORS (Hsu et al., 2011), which showed LacZ$^+$ cells in ~3% and ~30% of all HFs, respectively, at 2-day chase (Figures 1D, 1H, and S1B). Therefore, if Runx1-expressing cells of the ORS at early first catagen contribute to the "new" bulge and HG, we expected that, after 10-day chase (second telogen), a maximum of ~33% of HFs would contain LacZ$^+$ cells in the "new" bulge and HG. This appears to be the case for HG, because we found ~30% of HFs with LacZ$^+$ cells in the HG at 10-day chase (Figures 1E, 1F, and 1I).

Surprisingly, ~80% of HFs were labeled in the "new" bulge at 10-day chase, suggesting additional contribution from other HF compartments besides the ORS and "old" bulge (Figure 1I, left). The bulge has two layers: the outer layer containing SCs and the inner layer serving as the SC niche (Hsu et al., 2011). To distinguish these, we analyzed thin (20 μm) sections, and indeed, we found that only ~20% of HFs in thin sections (corresponding to ~30% of full HFs in thick sections) had LacZ$^+$ cells in the outer-bulge SC layer (Figures 1F and 1I, right), as expected from their known origin in the ORS. These data confirm that, in addition to contribution to HG, Runx1$^+$ ORS cells contribute to the new bulge. LacZ$^+$ cells were present in the inner bulge in ~50% of HF in thin sections, which corresponds to ~80% of full HFs in thick (60 μm) sections (Figures 1F, 1G, and 1I, right panel), the inner-layer LacZ$^+$ cells most likely originated in Runx1$^+$ HF TDL. Moreover, additional data suggest that Runx1$^+$ORS cells also contribute to new bulge and germ in the first telogen (Figures S1C and S1D), indicating that the same reorganization of the SC niche might take place repeatedly during homeostasis.

Endogenous Runx1 Expression Is Downregulated in the Hair Germ as It Begins Proliferation to Make the Matrix at Anagen and Upregulated in Apoptotic Matrix Cells

These data raised the possibility that Runx1 upregulation in the migrated bulge cells in early catagen ORS that act as precursors of the HG may promote a bulge-fate transition toward HG cells. Conversely, Runx1 downregulation in the ORS cells that returned to the "new" bulge may revert them to a bulge fate. To further investigate this, we first extended our previously reported analysis of Runx1 expression (Osorio et al., 2008) in bulge SC, HG EP, and

Figure 1. Runx1$^+$ Cells in the ORS at Catagen Generate New Bulge and Hair-Germ Cells

(A) Cartoon representation of cellular dynamics in the hair follicle shows the bulge SCs displaced into the outer root sheath (ORS) at late anagen/early catagen, which survive apoptosis and return upward to form the new bulge and the HG.

(B) Skin sections stained for Runx1 and bulge SC marker CD34 show cells in the ORS with low CD34 and high Runx1 expression starting at catagen II to III. Regions of the ORS with Runx1/CD34 overlap are enlarged in the upper right corner (white box). Note that Runx1 is upregulated in the most bulge-proximal CD34$^+$ ORS cells that lost contact with the inner layer. The ORS on the bulge side is made of cells placed immediately right of the dotted yellow lines.

(C) Scheme of tamoxifen (TM) injection to genetically label and trace Runx1-expressing cells from early catagen to telogen.

(D and E) Thick sections encompassing full hair follicles (HFs) stained with X-Gal to detect LacZ$^+$ cells.

(F and G) Same as (D) but in thin sections counterstained with hematoxylin to delineate the inner and the outer bulge layers.

(H and I) Counts of LacZ$^+$ HFs with distribution of label in each compartment. For abbreviations, see (A).

Error bars were calculated as SD using Excel.

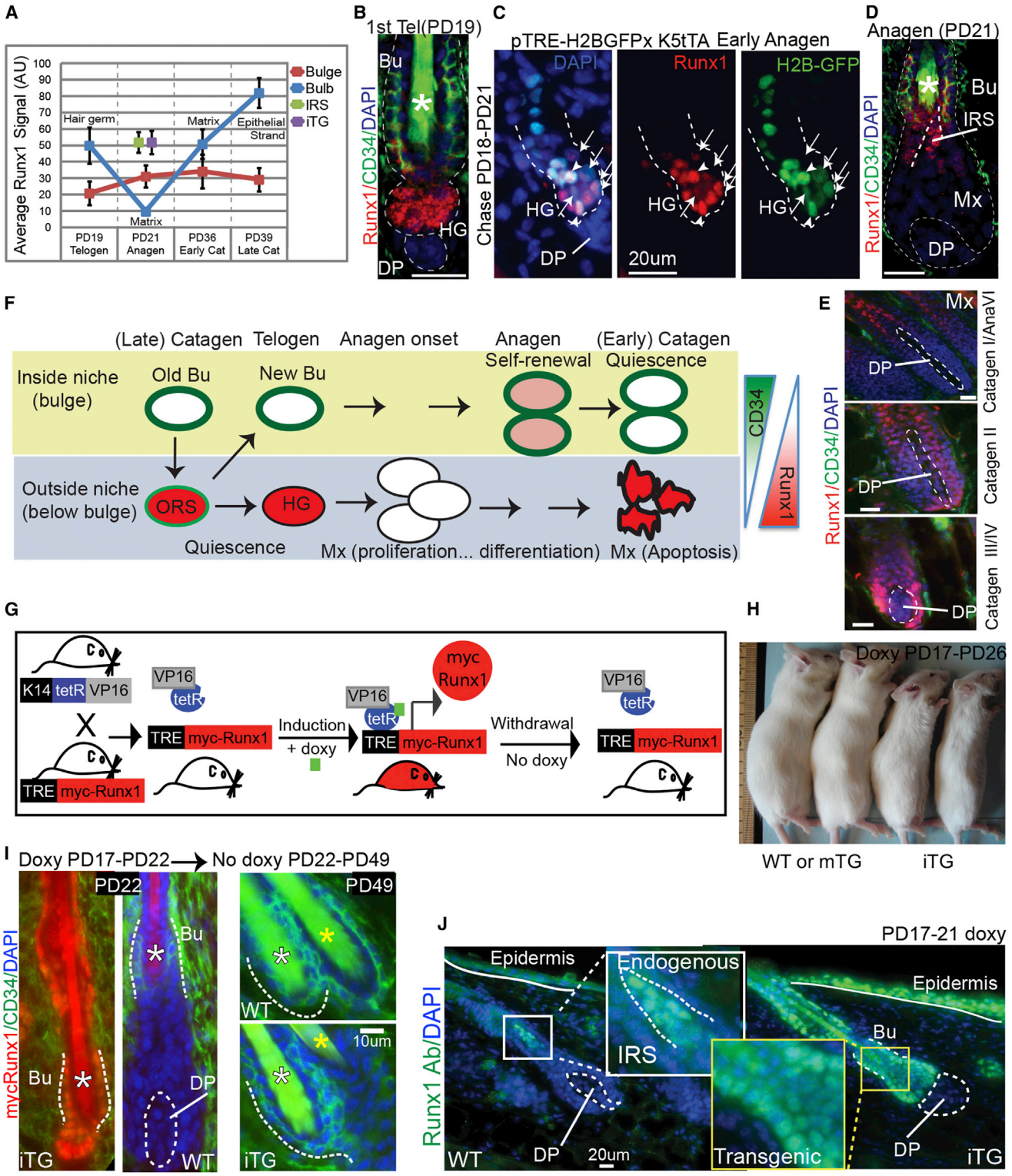

Figure 2. Transgenic Mouse to Model Runx1 Dynamic Expression Levels throughout the Hair Cycle

(A) Quantification of endogenous Runx1 levels throughout the hair cycle using immunofluorescence microscopy. See also Figures S1A, S1A′, and S1B. Data in purple represent the Runx1 levels quantified in the transgenic mouse model described in (G)–(J). a.u., arbitrary units.

(B, D, and E) Skin sections stained for endogenous Runx1 and CD34 show abrupt downregulation of Runx1 in the transition from the hair germ (HG) to the matrix (Mx) at anagen followed by upregulation in matrix and lower bulb cells at catagen.

(legend continued on next page)

matrix TA cell compartments throughout the hair cycle. Quantification of Runx1 protein by immunostaining revealed striking changes in levels in different compartments (Figures 2A, S1A, and S1A′).

In the bulge, Runx1 protein levels are generally low (Figure 2A), although necessary for normal bulge proliferation at anagen (Hoi et al., 2010). The mRNA level is higher in dividing bulge-sorted cells compared to nondividing bulge-sorted cells (Figure S2A, two asterisks). Bulge cells migrated in the upper ORS at catagen (Figures 1B and 2A) and, at the bulge/HG junction at telogen, express higher Runx1 protein levels (Osorio et al., 2008; Figure 2B).

In the HG, Runx1 is necessary for proliferation presumably by downregulating cyclin-dependent kinase inhibitors (Hoi et al., 2010; Lee et al., 2013; Osorio et al., 2008). Thus, we expected that Runx1 would remain high in dividing HG cells at anagen onset. Surprisingly, some HG cells with reduced H2B-GFP retention after 3-day doxycycline chase on TRE-H2BGFP;K5-tTA mice at anagen onset, indicative of one to two divisions (Zhang et al., 2009), showed reduced Runx1 protein and mRNA levels (Figures 2C, arrows, and S2A, one asterisk). The expression profiles of these divided HG cells at anagen onset resemble the matrix signature (Zhang et al., 2009), whereas the profiles of quiescent HG cells at telogen (prior to divisions) resemble the bulge (Greco et al., 2009). These observations suggest that, as HG EPs begin to divide, they rapidly transit to matrix TA cells and that Runx1 levels quickly decrease during this transition.

In the matrix, Runx1 protein remained undetectable throughout anagen but became suddenly high in early catagen, when these cells are known to undergo apoptosis (Figures 2A, 2D, 2E, S1A, and S1A′). Runx1 levels in matrix cells increased even more as catagen progressed and reached its highest level in the regressing apoptotic epithelial strand in late catagen (Figures 1B, 2A, S1A, and S1A′). This provides a strong correlation between Runx1 levels of endogenous expression and apoptosis in the matrix.

The dynamics of endogenous Runx1 expression are summarized in Figure 2F.

Generation of Tet-Inducible Transgenic Mice to Modulate Runx1 Expression Levels

To directly test a potential role of observed endogenous Runx1 level changes in the hair cycle, we generated tetracycline-inducible transgenic mice. The K14-rtTA construct ("on" in skin and other epithelia) will drive a newly generated TRE-mycRunx1 allele (see Experimental Procedures; Supplemental Information) upon doxycycline (doxy) induction. The K14-rtTA mice previously drove physiologically meaningful levels of another transcription factor in the skin (Nguyen et al., 2006). Within 4–6 hr of doxy induction, mycRunx1 expression would turn on, whereas withdrawing doxy would revert expression to undetectable levels (Figure 2G).

As expected, the doxy-induced TRE-mycRunx1;K14-rTA double transgenic mice (Figures 2H and S2B) turned on mycRunx1 nuclear expression, as shown by anti-myc staining (Figures 2I and S2C). Withdrawing doxy food shut down mycRunx1 expression by PD49 (Figure 2I, right). Two TRE-mycRunx1 mouse lines proved fully inducible by staining of different body regions (not shown), and we refer to them here as Runx1^{iTG}. Two mouse lines showed mycRunx1 expression in skin patches throughout the mouse back skin, and we refer to them here as mosaic Runx1^{mTG} lines. Double transgenic (TRE-MycRunx1;K14-rtTA) littermates without doxy and all single transgenic littermates showed no detectable staining and are designated as wild-type (WT) (Figures 2I and S2C). Runx1^{iTG} mice began losing weight 6 days after doxy induction (Figure 2H) and died within 9–12 days, but they recovered if we withdrew doxy food after 5 days of induction (Figure 6B). Runx1^{mTG} mice were viable, and we used them for long-term studies along with skin transplants from Runx1^{iTG} (Figures 2H, 4B, and 4C). All the experiments shown here were performed at least twice with $n_{mouse} \geq 2$ to 3 of each genotype per experiment.

To achieve near-physiological Runx1 protein levels and avoid artifacts of excessively high expression, we chose the doxy concentration of several tested (Experimental Procedures) that gave us consistently detectable mycRunx1 expression in the bulge, which appeared comparable to endogenous Runx1 expression in the IRS, HG, and early catagen matrix (Figure 2J, quantified in Figures 2A and S1A′).

Runx1 Is Insufficient for Anagen Onset but Sufficient to Induce Catagen

Runx1 is necessary for HG activation and proliferation and for timely anagen onset (Osorio et al., 2008), so we tested whether forced expression of Runx1 was sufficient to induce anagen. We induced Runx1^{iTG} during the second telogen, a period of prolonged quiescence in most mouse strains, but found no evidence of anagen onset, as shown by normal telogen morphology (Figures 3A and 3F, blue) and lack of bromodeoxyuridine (BrdU) staining in Runx1^{iTG} skin (Figure S2D). These results may suggest that the presence of inductive anagen signals, not present in the skin at second telogen, might be required in addition to Runx1 for normal anagen onset. Forced Runx1 expression in second telogen did, however, result in CD34 downregulation (Figure S4C).

We next induced mycRunx1 elevation in the short and synchronous first quiescence period (PD17∼PD20) where the anagen proliferative signals arise shortly after (PD20∼PD21). We doxy-fed Runx1^{iTG} mice for 4 to 5 days starting in quiescence at PD17 or PD19 and examined the HF morphology in skin sections stained with hematoxylin and eosin (H&E) (Figures 3B and 3F, red). In this Fvb mouse strain, WT skin was already at almost

(C) Skin sections from TRE-H2BGFP;K5-tTA mice doxy chased (PD18–PD21) show cells with an apparent inverse correlation between H2BGFP and Runx1 levels (arrowheads indicate undivided cells, whereas arrows point to cells that divided and diluted H2BGFP during the 3-day chase). Note the apparent Runx1 downregulation in divided HG cells. See also Figure S2A for mRNA levels in divided versus undivided cells isolated by FACS.
(F) Cartoon summarizing Runx1 expression levels in different compartments throughout the hair cycle.
(G) Scheme of transient mycRunx1 induction and withdrawal in transgenic mice responsive to doxy.
(H) Mice induced for 9 days with doxy are small and die within a few days. mTG mice are normal size and survive.
(I) Skin sections from WT and Runx1^{iTG} at stages indicated stained for mycRunx1 and CD34.
(J) Skin sections stained side by side for Runx1 and photographed at the same exposure. Note comparable transgenic Runx1 levels in the bulge (Bu) and HG to endogenous levels in the forming IRS quantified in (A) and Figure S1A′. See Figure 1A for abbreviations.
Error bars were calculated as SD using Excel.

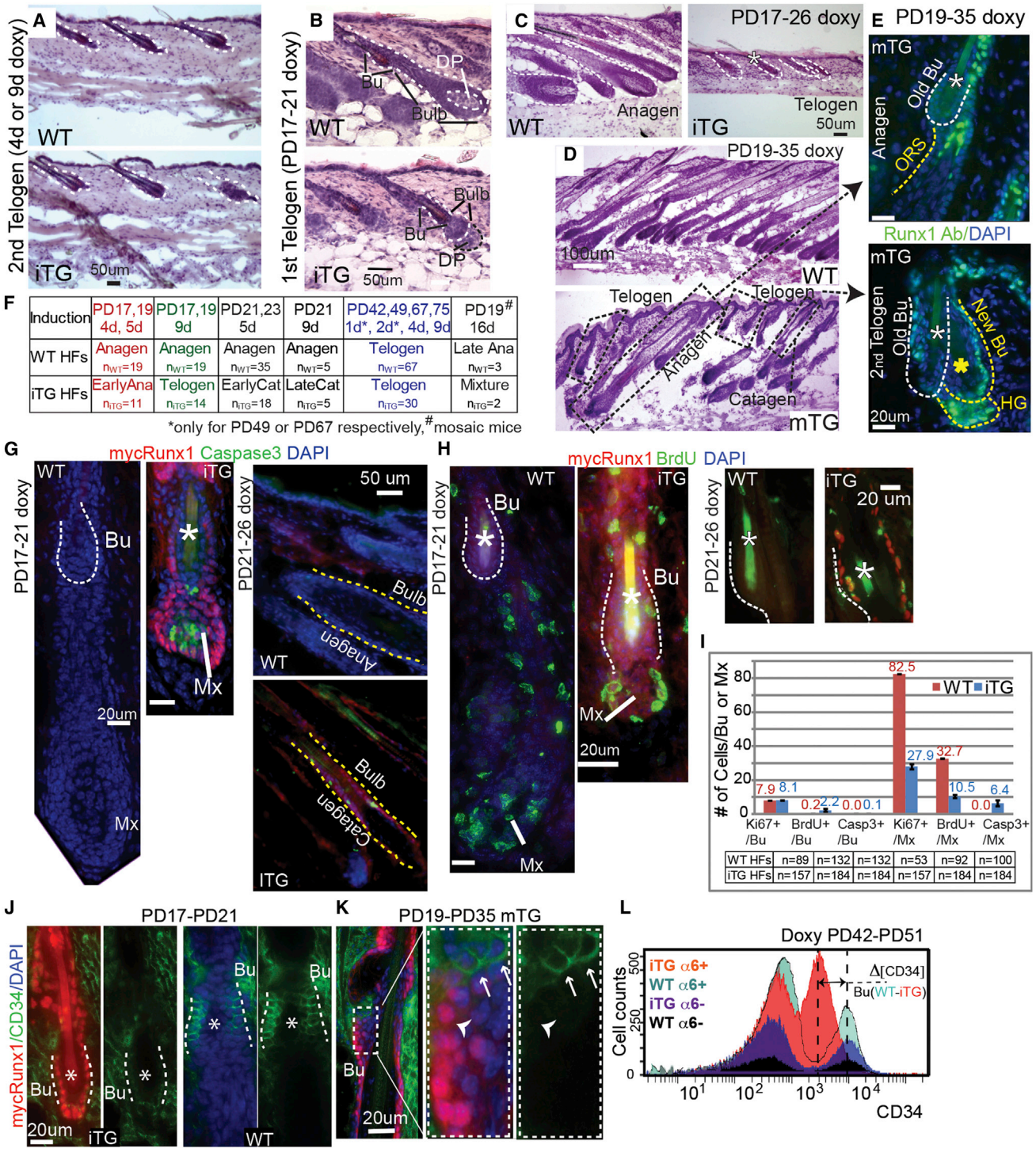

Induction	PD17,19 4d, 5d	PD17,19 9d	PD21,23 5d	PD21 9d	PD42,49,67,75 1d*, 2d*, 4d, 9d	PD19# 16d
WT HFs	Anagen n_{WT}=19	Anagen n_{WT}=19	Anagen n_{WT}=35	Anagen n_{WT}=5	Telogen n_{WT}=67	Late Ana n_{WT}=3
iTG HFs	EarlyAna n_{iTG}=11	Telogen n_{iTG}=14	EarlyCat n_{iTG}=18	LateCat n_{iTG}=5	Telogen n_{iTG}=30	Mixture n_{iTG}=2

Figure 3. Runx1 Expression Is Sufficient for Catagen Implementation in Bulb Cells but Requires Additional Anagen-Inductive Signals to Promote Stem Cell Proliferation

(A–D) Hematoxylin and eosin (H&E)-stained skin sections from doxy-induced mice at stages indicated. WT were littermate controls. Note normal telogen morphology in Runx1^{iTG} and WT in (A). Note Runx1^{iTG} HFs with smaller bulb and lack of hair shaft indicative of earlier anagen, with a DP unenclosed by the epithelial cells in (B) followed by return to telogen with a single hair shaft (*) in (C). (D) HFs in the 16-day induced mosaic Runx1^{mTG} skin showed variable hair-cycle stages (dotted rectangles).

(E) Corresponding stages are shown, with Runx1 antibody (Ab) staining (green). Note endogenous Runx1 expression pattern in anagen HF (top) and transgenic pattern (with a positive Bu and interfollicular epidermis) in late catagen/telogen HF (bottom). Note the presence of two hair shafts (*) indicating this

(legend continued on next page)

full anagen by PD21, showing a developed bulb and a newly forming hair shaft (Figure 3B, top). Contrary to our expectation that anagen would be accelerated, Runx1^{iTG} HFs were behind in anagen progression by 4 days of induction relative to controls (Figure 3B, bottom) and prematurely returned to telogen without producing a new hair shaft by 9 days (Figures 3C and 3F, green). Mosaic Runx1^{mTG} induced for 16 days at PD19 showed an abnormal mixture of different HF-cycle stages (Figures 3D and 3F, #). HFs at morphological stages comparable with WT littermates (anagen) showed the endogenous Runx1 staining pattern (Figure 3E, top). In contrast, HFs that expressed Runx1 at elevated levels in a transgenic pattern were found prematurely at catagen or the second telogen, as indicated by HF morphology and the presence of two hair shafts (Figure 3E, bottom). We attribute this phenotype to the misexpression of Runx1, not only in the quiescent bulge but also in the matrix and the lower ORS, where endogenous Runx1 is normally not expressed during anagen until these cells begin apoptosis at catagen onset.

Runx1^{iTG} induction for 5 and 9 days in early- and midanagen (PD21 and PD23) resulted in catagen morphology (Figure 3F, black, 3G, right panel, and S3C). This suggested that Runx1 is sufficient to induce catagen at any stage of anagen and may explain why endogenous Runx1 is suddenly turned on at its highest levels in the lower bulb in catagen.

Terminal differentiation markers analysis (GATA3 for the IRS and AE13 for the hair shaft) revealed complete lack of TDL in Runx1^{iTG} HFs induced at PD17/PD19 (Figure S3A). Apoptosis (caspase-3) and proliferation (BrdU injection 2 hr prior to sacrifice) analysis revealed massive apoptosis in the matrix (Figure 3G and S3C).

In the bulge, mycRunx1 downregulated CD34 (Figures 3J–3L and S4) and also increased proliferation (Figures 3H and S3B); the latter we expected would occur in conjunction with inductive proliferative signals present in skin at the first (short) telogen. CD34 reduction was cell autonomous, as suggested by mosaic analysis (Figure 3K), which ruled out a hair-cycle stage effect of Runx1 on bulge-marker CD34 expression. Quantification of BrdU, Ki67, and caspase-3 for the PD17–PD21 induction is provided in Figure 3I. Note that the difference in hair-cycle stage observed here cannot account for the differences in BrdU incorporation. This result implied that Runx1 elevation might promote the bulge-cell transition to a HG-like cell state as defined by being CD34− and more responsive to proliferative anagen-inducing signals present in the skin at the first telogen.

To distinguish direct versus systemic effects, we induced mycRunx1 expression in TRE-mycRunx1;K14-rtTA keratinocyte cell lines and in transiently transfected CD34^{+}/α6^{+} bulge and CD34^{-}/α6^{+} nonbulge sorted cultured cells (Figures S3D–S3F). Runx1 elevation resulted in a brief burst of BrdU incorporation, followed by a plunge below WT control levels, accompanied by increased apoptosis (Figures S3E and S3F). These data demonstrate a cell-autonomous effect on apoptosis and proliferation of keratinocytes by high Runx1 levels.

Long-Term Functional Assays Show that Stem Cells with Continuous High Runx1 Expression Switch to a Short-Lived Progenitor Behavior

Next, we performed long-term functional assays to ask if mycRunx1-expressing bulge cells continue to behave in vivo and in vitro like long-lived SCs or switch to a short-lived EP cell behavior.

We employed both skin grafts of the Runx1^{iTG} mice onto nude mice to avoid lethality after 9-day induction and the two Runx1^{mTG} mouse lines, which appeared healthy in long-term induction. Transplanted nude mice were fed doxy chow at the equivalent PD19, after shaving the original hair coat, which permanently arrested new hair coat growth (Figures 4A and 4B). Both Runx1^{mTG} mice and grafted Runx1^{iTG} skin began to lose the hair coat (in patches for Runx1^{mTG}) within a few weeks of induction and remained bald for the entire ~1-year duration of the experiment (Figures 4A–4C). Upon inspection of sections from the long-term Runx1^{iTG} skin, rare degenerated HF remnants were detected in Runx1^{iTG} dermis, which showed epithelial K14 expression but lacked the SC marker CD34 (Figure 4D). Thus, long-term expression of mycRunx1 in the HF in vivo inhibited the long-lived regenerative potential of bulge SCs and resulted in complete loss of the hair follicle, thereby causing a behavior expected of short-lived progenitors.

Next, we turned to colony formation assays (CFAs), an in vitro functional measure of self-renewal ability (Blanpain, 2010). Bulge SCs are slow in seeding colonies, but then they expand continuously whereas HG cells are fast in seeding colonies but shortly exhaust their growth potential (Greco et al., 2009). Primary keratinocytes isolated from Runx1^{iTG} skin of 5-day doxy-fed adult mice (PD17–PD22) displayed rapid initial proliferation with increased colony number and size, followed in ~40 days by exhaustion and cell senescence, being mostly lost from the dish by ~60 days (Figures 4E–4G and S6A–S6C), therefore behaving as short-lived HG EPs. As expected, WT cells showed the typical growth pattern of adult skin keratinocytes exhibited by long-lived SCs (Figures 4E–4G and S6A–S6C).

High Runx1 Expression in Bulge Cells Promotes a Massive Change in Gene-Expression Signature that Largely Resembles the Early Progenitor Hair Germ

Next, we analyzed the gene expression changes that occur in bulge cells upon mycRunx1 induction to further test if the bulge

HF had been through at least a portion of the first adult anagen. White asterisk marks the old shaft (club hair) in the old bulge, and yellow asterisk marks the new shaft.

(F) Summary of short-term doxy induction and results.

(G–I) Staining for markers indicated and quantified in (I) reveal increased BrdU incorporation (2 hr pulse) in Runx1^{iTG} bulge (Bu) and massive apoptosis in the matrix (Mx) and bulb.

(J and K) Skin sections from Runx1^{iTG} and Runx1^{mTG} mice show downregulation of CD34 by immunostaining. Note mosaic expression of mycRunx1 in bulge (Bu) in (K), correlating with lack of CD34 expression.

(L) FACS histogram shows overlay of four populations isolated from Runx1^{iTG} and WT littermate mouse skin when bulge SCs were at catagen/telogen. Note several-fold decrease in CD34 level in CD34^{+}/α6^{+} Runx1^{iTG} bulge cells compared to WT bulge. See also Figures S3 and S4.

Error bars were calculated as SD using Excel.

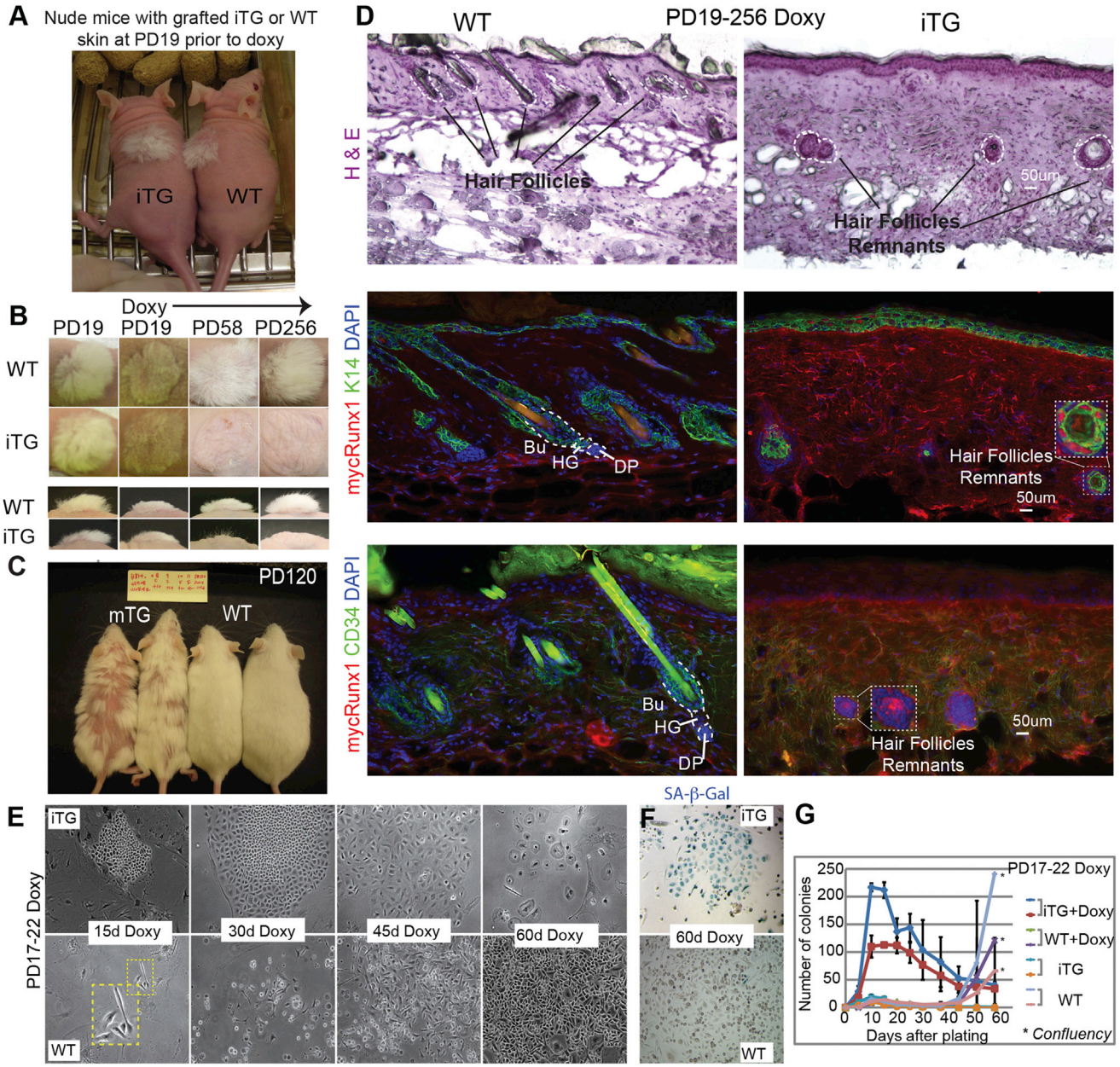

Figure 4. Long-Term Runx1 Induction in Bulge SCs Confer a Short-Lived Progenitor Cell Behavior Both In Vivo and In Vitro

(A) Grafted newborn Runx1^{iTG} skin onto nude mice, to bypass lethality of Runx1 induction, prior to doxy feeding at the equivalent PD19.

(B) Grafted areas on nude mice at times postinduction as indicated. Note permanent hair loss in Runx1^{iTG} skin.

(C) Runx1^{mTG} mice induced with doxy for >3 months show permanent hair loss in a patchy manner, as expected from mosaic expression of Runx1.

(D) Skin sections from (B) sectioned and stained as indicated show lack of HFs in Runx1^{iTG} skin. Circles show rare remnants of HF cells, which are stained positive for mycRunx1 and K14, but are negative for the SC marker CD34. MycRunx1 staining shows higher dermal background in Runx1^{iTG} than WT, possibly due to increased cellularity in the former.

(E–G) Keratinocytes isolated from PD17–PD22 doxy-treated mice were plated on irradiated mouse embryonic fibroblast in low Ca^{2+} E medium. Colonies were counted every week; representative phase contrast images are shown in (E) and the overall counts are shown in (G). See also Figures S6A and S6B. Note diminished colony size and flat-cell morphology indicative of senescence at 60 days in Runx1^{iTG} cells. (F) Endogenous SA-β-Gal staining indicates senescence of Runx1^{iTG} cells by 60 days. See also Figure S6C.

Error bars were calculated as SD using Excel.

cells are converting to a HG expression signature. Supporting this, the mRNA of CD34 and several other known HF SC markers was downregulated in the Runx1^{iTG} CD34^{+}/α6-integrin^{+} bulge cells, sorted within 1–5 days of doxy induction (Figures 5A and 5A′).

To examine global gene-expression changes we turned to Affymetrix microarrays. K15-EGFP mice (Morris et al., 2004) showed bright GFP expression in the HG and in some bulge cells at telogen (Figures 5B and 5C). Runx1^{iTG};K15-EGFP mice and WT;K15-EGFP control littermates were doxy-induced at ~PD19 for 1 day, and their skin cells were isolated by fluorescence-activated cell sorting (FACS) as CD34^{+}/α6^{+} bulge cells irrespective of GFP expression and as CD34^{-}/α6^{+}/GFP^{+} HG cells (Figures 5B and 5C). We examined skin from six different regions of the body to ensure telogen morphology and quiescence of bulge cells in all skin samples used for microarrays (Figures S5A and S5B). Affymetrix microarrays and GeneSpring software analysis revealed that over 2,500 probe sets (~2,500 genes) changed expression in Runx1^{iTG} bulge relative to WT bulge cells, suggesting profound and rapid changes in the molecular signature of quiescent bulge cells upon Runx1 elevation after only 1 day (Tables S1 and S2; Gene Expression Omnibus [GEO] database GSE53077 [National Center for Biotechnology Information number 16928442]).

Next, we compared the WT databases and extracted a bulge (4,453 probe sets) and a HG (2,556 probe sets) signature, as genes increased by >2× in one population versus the other (Tables S1 and S2). We used previously published databases to define the matrix signature, which was different from both the HG and bulge (Greco et al., 2009; Lien et al., 2011). Consistent with the known role of Runx1 in both activating and repressing transcription, 1,527 probe sets were downregulated in CD34^{+}/α6^{+} Runx1^{iTG} bulge compared to WT bulge cells and 1,097 probe sets were upregulated (Figure 5D). Importantly, the "bulge signature genes" were largely downregulated whereas the "HG signature genes" were largely upregulated in Runx1^{iTG} bulge compared to WT bulge (Figures 5E and S5C). A comparison with the matrix signature did not show a meaningful correlation with changing Runx1 levels (Figure 5E, right). These data strongly suggest that short-term induction of high Runx1 levels in quiescent bulge cells turns the molecular signature of bulge cells into that of a cell-state resembling HG cells.

To understand how Runx1 might act in quiescent bulge cells to promote a HG fate, we examined known pathways that regulate hair growth and homeostasis (Lee and Tumbar, 2012). However, these pathways were represented broadly among Runx1 target genes and did not suggest a single mode of action in this fate conversion (Table S2). Consistent with a role of Runx1 as master regulator of many pathways in a fate switch, a number of chromatin-remodeling factors, which are generally known to promote and stabilize cell-fate transitions, changed their mRNA expression (Figure S5D). The overrepresented Gene Ontology (GO) categories among downregulated bulge-signature genes were signal transduction, development, differentiation, cell motility, and cell adhesion (Figure 5F; Table S3; Supplemental Information). Conversely, the GO categories overrepresented among the upregulated HG-signature genes were all implicated in metabolism (Figure 5G; Table S3; Supplemental Information [see Discussion]).

The HG-like Cell State Induced by High Runx1 Levels in Bulge SCs Is Reversible

All the data so far suggest that endogenous Runx1 expressed in bulge SCs migrated in the ORS at catagen may promote the early steps of SC differentiation toward early progenitor HG fate. Because some of these Runx1^{+} ORS cells return to the "new" bulge, lose Runx1 expression, and regain CD34, we wondered whether the HG-like state induced by Runx1 in ORS cells might be functionally reversible. To test this, we doxy-fed Runx1^{iTG} mice for 5 days starting at PD17 (or PD21) to express mycRunx1 and induce the HG-like cell state in bulge cells, followed by doxy withdrawal (Figure 6A). These mice are now designated as Runx1$^{iTG,\ withdrawn}$. After >23 days of doxy food withdrawal, mycRunx1 expression was no longer detectable (Figure 2I). Whereas bulge CD34 expression is lost upon 1–5 days of mycRunx1 expression (Figures 3J–3L, S4A, and S4B), it was fully restored in Runx1$^{iTG,\ withdrawn}$ mice by PD49 (Figure 2I).

We then monitored hair growth, lineage contribution, and cell-culture behavior to examine if bulge cells that experienced transient high Runx1 levels can return to a SC phenotype (Figure 6A). In marked contrast to Runx1^{mTG} mice or skin grafts from Runx1^{iTG} mice, in which long-term mycRunx1 expression led to HF and SC loss, hair growth in Runx1$^{iTG,\ withdrawn}$ mice showed a slight delay in the first anagen onset but then cycled normally for two additional hair cycles (Figure 6B).

Next, we examined the lineage contribution of the WT and Runx1$^{iTG,\ withdrawn}$ bulge SCs to verify that they self-renew and differentiate in a similar manner, despite the transient Runx1 expression in the latter. Thus, we performed lineage-tracing experiments using quadruple Runx1-CreER;Rosa26R-LacZ; Runx1^{iTG} (TRE-mycRunx1;K14-rtTA) transgenic mice. We first marked bulge cells by TM injection at PD17 (catagen) and then induced mycRunx1 expression by feeding mice doxy food at PD21. Subsequent tracking of marked Runx1$^{iTG,\ withdrawn}$ bulge SCs and their progeny showed no difference in LacZ^{+} cell distribution and frequency within the bulge (indicating self-renewal) or bulb (indicating differentiation) compared to WT bulge cells (Figures 6C–6E and S7). Thus, the bulge SCs that had functionally behaved as HG cells after Runx1 level elevation reverted to a normal SC behavior, self-renewing and differentiating over long term at similar rates with the WT bulge cells upon doxy withdrawal.

To further test the reversibility of the cell state induced by transient Runx1 expression in bulge SCs, we also performed in vitro functional assays (Figure 6F). Keratinocytes isolated from PD79 Runx1$^{iTG,\ withdrawn}$ mice (but not earlier) showed normal SC-like patterns of colony formation, like the WT controls (Figure 6G). In contrast, if we added doxy to Runx1$^{iTG,\ withdrawn}$ cells in culture, they behaved again as early progenitor HG-like cells (Figure 6G; iTG; withdrawn+doxy). All these functional assay data were consistent with reversion of HG-like fate induced by Runx1 to a bulge SC fate upon Runx1 withdrawal.

DISCUSSION

With this work, we examined the role of changing endogenous Runx1 levels throughout the hair cycle, which appears to be specialized in different HF compartments. We propose that

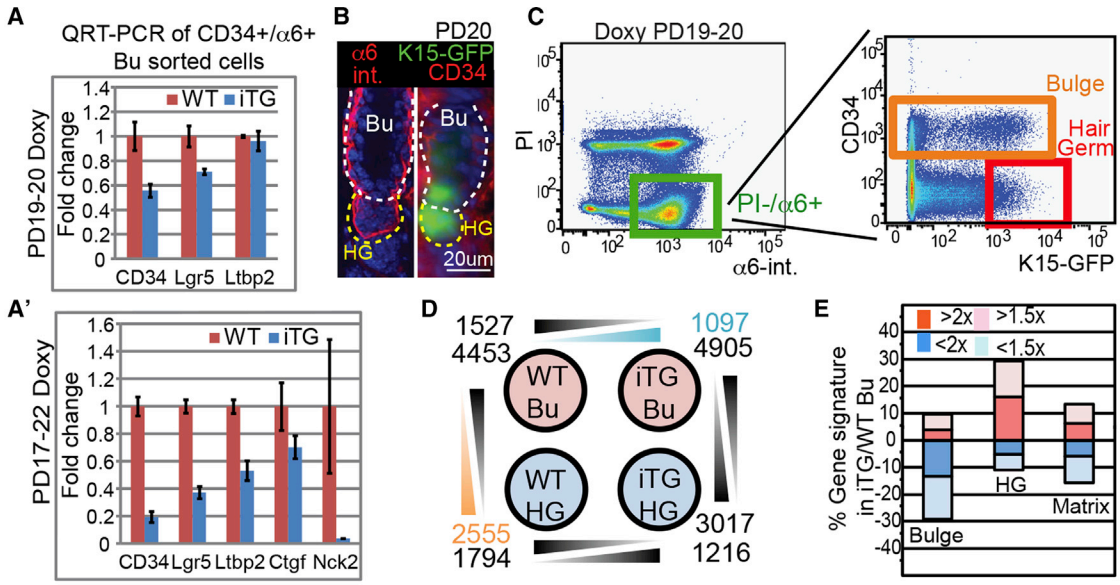

F

GO Categories Enriched in Bu Genes Downregulated in iTG Bu (596 Probes)

Term	p value	Count	Fold Enrichment
GO Biological Process			
Integrin *binding/complex/-mediated signaling*	$2 \times 10^{-5}/3 \times 10^{-5}/3.5 \times 10^{-7}$	8/6/11	7/10/07
Adhesion *biological/cell/cell-cell/regulation of cell adhesion*	$4 \times 10^{-7}/4 \times 10^{-7}/4.5 \times 10^{-6}/2 \times 10^{-5}$	35/35/20/14	2.6/2.6/3.2/3.9
Migration *cell/cell motility/locomotion/component movement*	$9 \times 10^{-7}/5 \times 10^{-6}/1.5 \times 10^{-6}/1 \times 10^{-6}$	23/23/30/25	3.2/2.9/2.6/3.0
Signal transduction/Signaling	$4.5 \times 10^{-5}/2 \times 10^{-5}$	96/104	1.5/1.5
Development *anatomical structure/cell/cellular process/system*	$2 \times 10^{-5}/5 \times 10^{-5}/8 \times 10^{-5}/4 \times 10^{-5}$	88/35/67/79	1.5/2.0/1.5/1.6
Cell differentiation	4.00×10^{-5}	67	1.6
Neuron *projection morphogenesis*	9.00×10^{-5}	16	3
Protein *domain specific binding/polymerization*	$3 \times 10^{-6}/4 \times 10^{-5}$	27/7	2.7/7.3
GO Cellular Component			
Cytoplasmic microtubule	1.50×10^{-5}	6	10.8
Membrane */plasma membrane/cell periphery*	$5 \times 10^{-5}/6 \times 10^{-6}/4 \times 10^{-6}$	175/99/102	1.3/1.5/1.3

G

GO Categories Enriched in HG Genes Upregulated in iTG Bu (414 Probes)

Term	p value	Count	Fold Enrichment
GO Biological process			
Lipid *metabolic process/cellular metabolic/biosynthetic process*	$9.5 \times 10^{-10}/6 \times 10^{-7}/2 \times 10^{-6}$	40/28/20	3/3/3.4
Fatty acid *metabolic/biosynthetic process*	$1.5 \times 10^{-6}/6 \times 10^{-5}$	21/9	4./5
Catalytic activity	1.6×10^{-6}	129	1.4
Oxidoreductase activity/oxidation-reduction	$2 \times 10^{-6}/2.7 \times 10^{-6}$	32/35	2.5/2.3
Oxoacid metabolic process	2.00×10^{-5}	36	2.5
Carboxylic/Monocarboxilic acid metabolic/biosynthetic	$2 \times 10^{-5}/6.6 \times 10^{-8}/5.5 \times 10^{-5}$	26/21/13	2.5/4/3.7
Organic acid *metabolic process/biosynthetic process*	$2.5 \times 10^{-5}/5.5 \times 10^{-5}$	26/13	2.5/3.7
Cellular ketone metabolic process	2.9×10^{-5}	26	2.4

Figure 5. Runx1 Initiates a Hair-Germ, Early-Progenitor Fate in Bulge Cells

(A and A') Quantitative RT-PCR (qRT-PCR) of sorted bulge cells show robust downregulation of several bulge stem cell markers tested.

(B) Skin sections from K15-EGFP;Runx1^{iTG} mice at PD20 show telogen morphology and GFP expression in the HG and in some bulge (Bu) cells.

(C) FACS dot plot shows sorting gates to isolate bulge (as CD34^{+}/α6^{+}/GFP$^{+/-}$ cells) and HG cells as (CD34−/ α6^{+}/GFP^{+}). The cutoff for HG GFP was for the brightest 1/3 of the cells to avoid potential contamination from dimmer cells occasionally found in epidermis and sebaceous gland (not shown).

(D) Microarray analysis of wild-type (WT) and iTG-bulge (Bu) and hair-germ (HG)-sorted populations; shown are number and probes, which decrease or increase among each paired comparison.

(legend continued on next page)

Runx1 acts as a determining factor in the transition from bulge SCs to the early progenitor HG cell state. This state induced by Runx1 in quiescence is reversible and represents a metastable intermediate in the SC to TA cell-fate transition (Figure 7). Moreover, we found that Runx1 is sufficient for catagen induction in full anagen HF.

Runx1 Expression in Bulge Cells Promotes the Transition toward the Hair-Germ Fate

An important outcome of this study is that mycRunx1 elevation in bulge SCs induces significant changes in gene expression and cell behavior that closely resemble the HG EP fate. Previously, our candidate approach revealed Wnt, Stat3, and p21 as regulated downstream of Runx1 in the HF (Lee et al., 2013; Osorio et al., 2011; Scheitz et al., 2012). Here, we show that Runx1 broadly regulates bulge expression of ~2,500 genes that fit multiple pathways, including global-chromatin-remodeling factors. This is consistent with a probable role of Runx1 as one of the master regulators that switch off the bulge signature and on the HG gene signature. Moreover, whereas WT keratinocytes behave as SCs in culture, the mycRunx1-expressing keratinocytes adopt rapid proliferation and short-lived behavior typical of early progenitors, previously described for WT HG cells (Greco et al., 2009). In vivo, bulge cells with mycRunx1 expression initially proliferate faster in response to anagen signals but are lost from the skin in long term, therefore also behaving essentially as short-lived progenitors.

Previously, we have implicated Runx1 as a proliferation factor in HG and bulge-cell activation at anagen onset by loss of function studies (Osorio et al., 2008). Here, we carefully describe endogenous Runx1 levels, which appear tightly coupled with cell location relative to the bulge SC niche. Within the bulge, low Runx1 levels are apparently needed for normal bulge SC proliferation rates during anagen (Figure 7A; Hoi et al., 2010). Quiescent SCs outside the niche in the ORS at catagen exhibit elevated endogenous Runx1 levels that remain high as these cells form the HG at telogen and then decrease again right at proliferation onset as these HG cells become matrix TA cells (Figure 7B). Although Runx1 expression is necessary for HG and bulge-cell activation/proliferation and for anagen onset (Osorio et al., 2008), we find here by transgenic expression that it is not sufficient. Based on all these data, we propose that Runx1 endogenous expression in the ORS at quiescence (catagen/telogen) in bulge SCs transitioning toward HG may prepare these cells for overcoming their "slow-cycling" SC character, thus becoming fit for rapid response to subsequent proliferation signals, as expected of HG cells. This "fitness" is perturbed in the absence of Runx1, resulting in delay of SC activation.

Our gene-expression studies begin to reveal some of the potential specific functions Runx1 may be performing during the transition of bulge SC to the early progenitor HG. In particular, cell-adhesion genes are downregulated, suggesting that Runx1 might promote bulge-cell release from the niche and migration down the basement membrane into the ORS. Consistent with this interpretation, Runx1-deficient keratinocytes display defects in cell migration (Osorio et al., 2011). Conversely, HG signature genes preferentially upregulated by Runx1 in the quiescent bulge cells are metabolic enzymes. We previously showed that Runx1 promotes the G1/S transitions of the cell cycle in skin keratinocytes (Hoi et al., 2010). Therefore, a potential involvement of Runx1 in cell growth during the G1 phase in vivo, prior to divisions at anagen onset, may explain at least in part how Runx1 might act in G0/G1 quiescence during catagen to prepare HG cells for their subsequent proliferation at anagen onset. An interesting twist is that, even though ORS cells downregulate Runx1 upon entering the "new" bulge, their transient endogenous Runx1 expression in the ORS may also prepare them for the subsequent proliferation at anagen for proper SC self-renewal. These aspects of Runx1 regulation will be subject of a future study.

In summary, all our data suggest that the role of endogenous high Runx1 levels in ORS cells that migrated from the bulge at catagen is to promote the early steps of their fate transition toward the early progenitor HG.

Runx1 Expression in the Lower-Hair-Follicle Bulb Is Sufficient to Implement Catagen

Despite the highest endogenous Runx1 expression in the apoptotic bulb and epithelial strand at catagen (Figure 7E), our previous knockout studies did not reveal a role of Runx1 at this stage. Here, however, we show that early elevation of Runx1 can initiate apoptosis exclusively in those cells that would normally express high levels of Runx1 just as they begin to undergo apoptosis. Because the affected HFs progress through catagen to a normally structured telogen, we propose that expression of endogenous Runx1 is a normal trigger of apoptosis at catagen. However, there must be a redundant system(s) to trigger apoptosis in the absence of Runx1. Interestingly, endogenous high Runx1 expression at catagen below the bulge appears to conveniently couple the removal of the "used" matrix TA and TDL cells with the differentiation of bulge SCs toward supplying new HG early progenitors, making catagen an essential state cell-fate acquisition in HF.

Reversible Hair-Germ-like Cell State Induced by Runx1 in Quiescent Hair-Follicle Stem Cells during Normal Homeostasis

Whereas previous work demonstrated that "old" bulge cells that migrated into the upper ORS returned to the "new" bulge (Hsu et al., 2011), experimental evidence supporting significant functional and/or molecular changes during this journey outside the niche was lacking. Here, we provide expression and lineage tracing data demonstrating that the migrated bulge cells in the upper ORS upregulate endogenous Runx1 and downregulate it again when they return to the "new" bulge. Furthermore, we find that Runx1 upregulation in bulge cells rapidly promotes a

(E) Comparison of bulge iTG/WT by microarrays shows changes in bulge (Bu), hair-germ (HG), and matrix-gene signature. Note downregulation of bulge signature and upregulation of HG signature in iTG bulge. The effect on matrix signature was neutral. See also Figure S5C.
(F and G) GO categories enriched among Runx1 targets in two selected gene subsets, as indicated.
qRT-PCR signals for each gene were normalized to GAPDH, and errors of experimental conditions were propagated to calculate SD.

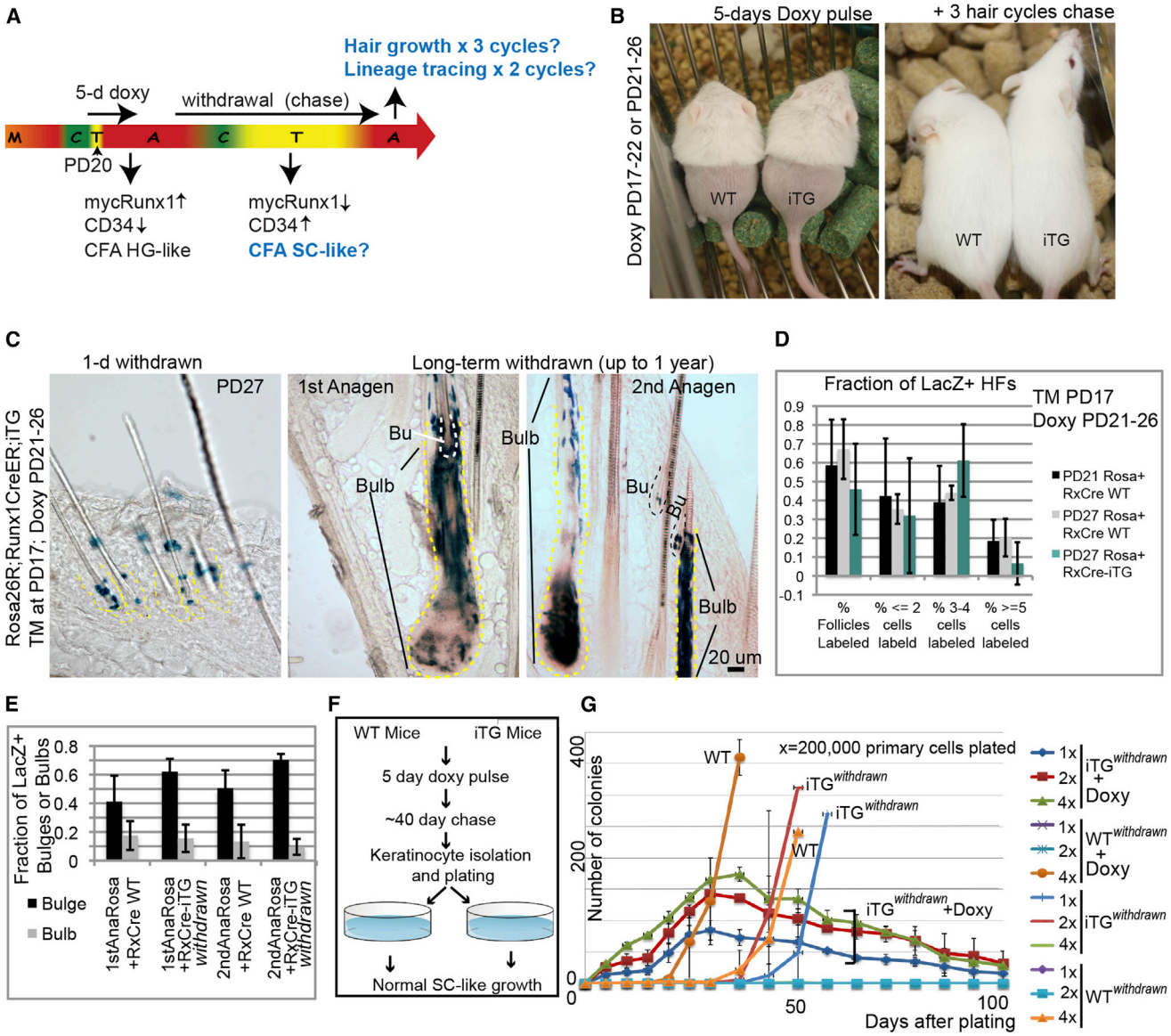

Figure 6. Bulge Stem Cell Fate Transition Induced by Runx1 Is Functionally Reversible

(A) Scheme of doxy induction and withdrawal to assess reversibility of Runx1-induced effects on bulge-cell function.

(B) Mice on doxy food (left) had hair on their lower backs gently removed to monitor hair growth without causing activation of growth by injury. They regrew hair after doxy withdrawal (right) for three consecutive cycles (compare with Figure 4B).

(C) Skin sections from Runx1-CreER;Rosa26R;Runx1^{iTG} mice injected with TM at PD17, doxy treated from PD21–PD26, and sacrificed at PD27 (left panel) show localization of LacZ$^+$ cells to the bulge. Middle and right panels show LacZ$^+$ cells in the differentiated HF compartment (bulb) and in the SC compartment (Bu) at the two subsequent anagen stages after TM injection.

(D and E) LacZ$^+$ HF counts of images collected from all stages in (C) show similar patterns of LacZ contribution to HF regeneration in iTG and WT skin. See also Figure S7.

(F) Scheme of doxy treatment and withdrawal for colony formation assays (CFA) to examine the growth potential (self-renewal ability) of cells that transiently experienced mycRunx1 expression.

(G) CFA of cells from (F) show recovery of SC-like behavior in cells from mice in which doxy was withdrawn for several weeks after the initial 5 days of doxy treatment (note iTG^{withdrawn} versus WT plots). Keratinocytes from these mice, cultured with doxy upon plating, displayed once again the behavior described previously for the HG (rapid proliferation followed by death; see plots marked iTG^{withdrawn} +doxy). See also Figure S7.

Error bars were calculated as SD using Excel.

cell state resembling the early progenitor HG (see the first section of the Discussion) and that this effect is functionally reversed when Runx1 is downregulated.

Dedifferentiation of the HG to bulge cells was previously proposed as a response to injury (hair plucking), although lineage-tracing data are still missing (Ito et al., 2004), and was also shown

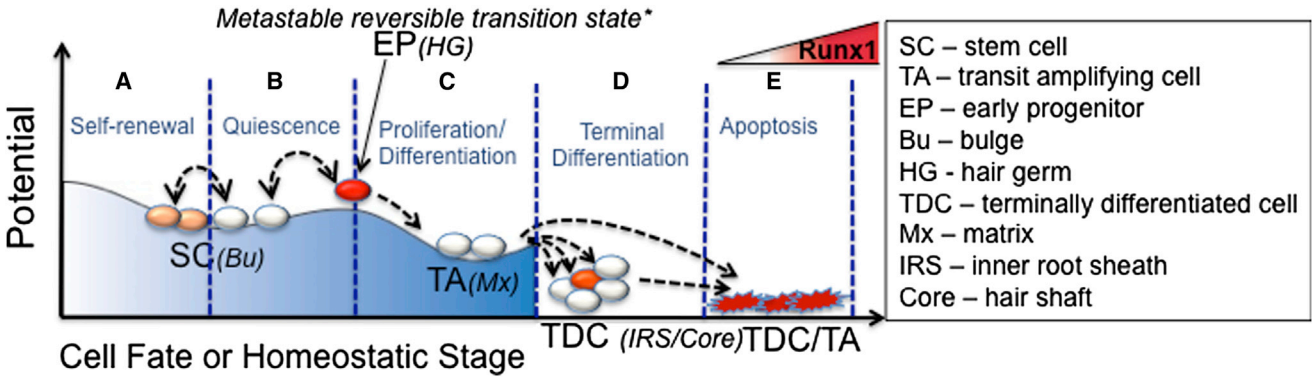

Figure 7. Proposed Role of Changing Levels of Runx1 in Adult Hair-Follicle Homeostasis

(A) Low levels of Runx1 expression in bulge cells enhance self-renewal (Hoi et al., 2010).

(B) Runx1 upregulation in quiescent bulge cells found outside the niche results in early progenitor fate, a metastable and reversible state, that functions as an intermediate between stem cells (bulge) and transit-amplifying cells (matrix).

(C) Inductive proliferation and differentiation signals cause the early progenitor to proliferate, downregulate Runx1, and fall down the hill of biological potential to a more stable (irreversible) matrix TA cell fate.

(D) TA cells terminally differentiate to specific HF lineages. Relatively high Runx1 expression in one (IRS) of these lineages during anagen is shown in red.

(E) TDC/TA cells with high Runx1 expression undergo apoptosis and therefore are plotted at zero potential. The reversible fate change induced by Runx1 is based on transgenic transient-expression experiments.

to occur in response to injury by LASER ablation (Rompolas et al., 2013). Our data suggest that differentiation and dedifferentiation of bulge SCs are likely to occur naturally at catagen, during the bulge SC journey outside the niche (old bulge) in the ORS followed by a return (new bulge), when these traveling SCs experience changing endogenous Runx1 levels. Moreover, these SC fate changes occur in the absence of cell division, because bulge and upper- and mid-ORS cells are known to withdraw from the cell cycle during this catagen/telogen period (Hsu et al., 2011). This flexibility in fate may provide robustness to produce the correct ratio of "new" bulge and "new" HG cells from a fixed pool of quiescent "old" bulge cells to recreate the proper telogen HF structure for the next regeneration cycle.

Lessons for Tissue Stem Cell Early Differentiation: Quiescent Reversible Transition State

Our data fit a model for HF SC fate determination that follows Ferrell's theory proposed for early development fate transitions (Ferrell, 2012), as an alternative to the irreversible fates described by Waddington (1957). Specifically, the first step in stem cell differentiation toward a progenitor cell may occur in quiescence (catagen/telogen), when some SCs exit the niche and become early progenitors (HG cells). The differentiation of SCs to TA or progenitor cells would occur through a reversible transition state, the "early progenitor," conveniently represented in the HF by an identifiable and sufficiently long-lived (although still short-term) cell state, the HG. SC differentiation into early progenitor cells is probably driven by upregulation of certain fate determinants, of which Runx1 appears to be an early one in the HF. The early progenitor transition state is metastable, as it would either fall backward from the hill of biological potential to remake SCs (when HG-like cells in ORS dedifferentiate to the "new" bulge) or fall forward to divide and make the TA cells (differentiation of HG cells to matrix cells), which are more stable cell states. Additional inductive proliferative signals (anagen promoting) are also needed for the early progenitors to engage in cell division and become TA cells (Figure 7F). The fate reversibility is likely to cease upon cell division, as suggested in the HF by the fact that dividing HG cells rapidly change to acquire matrix TA characteristics upon one to two divisions (Zhang et al., 2009), and matrix cells cannot make SCs, as shown by lineage tracing (Greco et al., 2009).

Our proposed model in the HF, which implicates a reversible transition cell state in quiescence mediating the SC to TA cell-fate commitment, may provide new insight especially to the SC systems that are more active or less synchronous than the HF, where the steps of SC to TA cell-fate transition are difficult to delineate and the EP transition state is very short-lived.

EXPERIMENTAL PROCEDURES

Mice

Mouse work followed Cornell Institutional Animal Care and Use Committee guidelines. The c-Myc tag was inserted to the Runx1 N terminus in the pcDNA3.1Runx1b (a gift from Nancy Speck), and the mycRunx1 fragment was transferred to pTRE2 (Clontech) vector. Cornell Mouse Transgenic Core Facility generated ten transgenic TRE-mycRunx1$^+$ mice, which were tested for inducibility by crossing with K14-rtTA mice (Nguyen et al., 2006) and feeding mice with 20, 60, 200, and 1,000 mg/kg mouse chow. The last concentration was used in all subsequent experiments. We used TRE-H2BGFP; K5-tTA for in vivo cell-division counting (Tumbar et al., 2004), Runx1-LacZ mice for Runx1 expression studies (North et al., 2002), and Runx1-CreER mice (Samokhvalov et al., 2007) crossed with Rosa26RLacZ mice (JAX) for lineage tracing. Sequential crosses were performed to obtain quadruple transgenic mice: Runx1-CreER;Rosa26LacZ;TRE-mycRunx1 (iTG, fully inducible);K14-rtTA. For hair-germ and bulge cell sorting after 1-day doxy induction at ~PD19, we crossed K15-EGFP mice (Morris et al., 2004) with TRE-mycRunx1(iTG);K14-rtTA mice.

Microarrays

Sorted CD34$^+$/α6$^+$ (bulge) and CD34$^-$/α6$^+$/GFP$^+$ (hair germ) cells were used to prepare mRNA from two different mice of each genotype and then subjected to Affymetrix microarray assay (Cornell Core Facilities) followed by GeneSpring

analysis. After excluding the probes with a signal value <100 or called absent, genes designated as on average ≥2-fold up in WT bulge versus WT HG (4,453 probes) and ≥2-fold up in WT HG versus WT bulge (2,555 probes) were defined as bulge and HG signature genes, respectively. The matrix signature genes were defined as ≥2-fold up in anagen matrix versus anagen bulge and telogen bulge, utilizing previously published databases (Lien et al., 2011).

Immunofluorescence Staining

The frozen-cut skin sections were incubated with primary antibodies in the blocking solution for 1–4 hr at room temperature or overnight at 4°C with following dilution: rabbit anti-Runx1 (1:4,000; a gift from Thomas Jessell), mouse anti-Myc tag (1:200; Zymed), rat anti-CD34 (1:50; BD Biosciences), rabbit anti-K5 or K14 (1:1,000; Covance), rabbit anti-activated caspase-3 (1:500; R&D Systems), mouse anti-AE13 (1:50; Immunoquest), mouse anti-AE15 (1:10; a gift from Tung-Tien Sun), mouse anti-GATA3 (1:100; Santa Cruz Biotechnology), rat anti-BrdU (1:300; Abcam), and rabbit anti-Ki67 (1:1,000; NovoCastra Laboratories). This was followed by incubation in secondary antibody fluorescently coupled with fluorescein isothiocyanate or Texas red.

Microscopy and Image Processing

We examined all stained samples under a fluorescent upright light microscope (Nikon). Images were obtained with a charge-coupled device 12-bit camera (Retiga EXi; QImaging) using the IP-Lab software (MVI), color combined, and assembled in montages. All the images were processed with Photoshop and Illustrator (Adobe) to enhance the contrast, brightness, and levels to the same extent among samples within the same experiment.

Cell Culture and Colony Formation Assay

Two hundred thousand live skins isolated in sterile conditions from adult mice were plated onto the embryonic feeder cell layers in low-Ca^{2+} keratinocyte E medium (Barrandon and Green, 1987). To maintain Runx1 expression, 0.5 μg of doxy/ml of media was added to cultures. The number of colonies was counted by phase-contrast microscopy every 5 days during the first 30 days and every 7 days during the last 30 days.

See also Supplemental Information for additional details on the procedures.

ACCESSION NUMBERS

The GEO accession number for the data reported in his paper is GSE53077.

SUPPLEMENTAL INFORMATION

Supplemental Information includes Supplemental Experimental Procedures, seven figures, and three tables and can be found with this article online at http://dx.doi.org/10.1016/j.celrep.2013.12.039.

ACKNOWLEDGMENTS

We thank Y. V. Zhang and C. M. Piskun for experiments in Figures 2C and S2A and many colleagues for reagents (see Experimental Procedures and Supplemental Information). The Cornell Cytometry core is supported in part by the Empire State Stem Cell Foundation (ESSCF), New York State-Department of Health (NYS-DOH), contract C026718. Opinions do not necessarily reflect the view of ESSCF, the NYS-DOH, or NYS. Funding was from New York Stem Cell Program C024354 and National Institutes of Health R01AR053201 to T.T. and Human Science Frontier to A.S. We thank colleagues, in particular M. Rendl (Mount Sinai) for constructive criticism and V. Vogt (Cornell) for moral support.

Received: August 16, 2013
Revised: October 31, 2013
Accepted: December 27, 2013
Published: January 23, 2014

REFERENCES

Barrandon, Y., and Green, H. (1987). Three clonal types of keratinocyte with different capacities for multiplication. Proc. Natl. Acad. Sci. USA *84*, 2302–2306.

Blanpain, C. (2010). Stem cells: Skin regeneration and repair. Nature *464*, 686–687.

Blyth, K., Cameron, E.R., and Neil, J.C. (2005). The RUNX genes: gain or loss of function in cancer. Nat. Rev. Cancer *5*, 376–387.

Ferrell, J.E., Jr. (2012). Bistability, bifurcations, and Waddington's epigenetic landscape. Curr. Biol. *22*, R458–R466.

Greco, V., Chen, T., Rendl, M., Schober, M., Pasolli, H.A., Stokes, N., Dela Cruz-Racelis, J., and Fuchs, E. (2009). A two-step mechanism for stem cell activation during hair regeneration. Cell Stem Cell *4*, 155–169.

Hoi, C.S., Lee, S.E., Lu, S.Y., McDermitt, D.J., Osorio, K.M., Piskun, C.M., Peters, R.M., Paus, R., and Tumbar, T. (2010). Runx1 directly promotes proliferation of hair follicle stem cells and epithelial tumor formation in mouse skin. Mol. Cell. Biol. *30*, 2518–2536.

Hsu, Y.C., Pasolli, H.A., and Fuchs, E. (2011). Dynamics between stem cells, niche, and progeny in the hair follicle. Cell *144*, 92–105.

Ito, M., Kizawa, K., Hamada, K., and Cotsarelis, G. (2004). Hair follicle stem cells in the lower bulge form the secondary germ, a biochemically distinct but functionally equivalent progenitor cell population, at the termination of catagen. Differentiation *72*, 548–557.

Jaks, V., Kasper, M., and Toftgård, R. (2010). The hair follicle-a stem cell zoo. Exp. Cell Res. *316*, 1422–1428.

Lee, J., and Tumbar, T. (2012). Hairy tale of signaling in hair follicle development and cycling. Semin. Cell Dev. Biol. *23*, 906–916.

Lee, J., Hoi, C.S., Lilja, K.C., White, B.S., Lee, S.E., Shalloway, D., and Tumbar, T. (2013). Runx1 and p21 synergistically limit the extent of hair follicle stem cell quiescence in vivo. Proc. Natl. Acad. Sci. USA *110*, 4634–4639.

Lien, W.H., Guo, X., Polak, L., Lawton, L.N., Young, R.A., Zheng, D., and Fuchs, E. (2011). Genome-wide maps of histone modifications unwind in vivo chromatin states of the hair follicle lineage. Cell Stem Cell *9*, 219–232.

Morris, R.J., Liu, Y., Marles, L., Yang, Z., Trempus, C., Li, S., Lin, J.S., Sawicki, J.A., and Cotsarelis, G. (2004). Capturing and profiling adult hair follicle stem cells. Nat. Biotechnol. *22*, 411–417.

Müller-Röver, S., Handjiski, B., van der Veen, C., Eichmüller, S., Foitzik, K., McKay, I.A., Stenn, K.S., and Paus, R. (2001). A comprehensive guide for the accurate classification of murine hair follicles in distinct hair cycle stages. J. Invest. Dermatol. *117*, 3–15.

Nguyen, H., Rendl, M., and Fuchs, E. (2006). Tcf3 governs stem cell features and represses cell fate determination in skin. Cell *127*, 171–183.

North, T.E., de Bruijn, M.F., Stacy, T., Talebian, L., Lind, E., Robin, C., Binder, M., Dzierzak, E., and Speck, N.A. (2002). Runx1 expression marks long-term repopulating hematopoietic stem cells in the midgestation mouse embryo. Immunity *16*, 661–672.

Osorio, K.M., Lee, S.E., McDermitt, D.J., Waghmare, S.K., Zhang, Y.V., Woo, H.N., and Tumbar, T. (2008). Runx1 modulates developmental, but not injury-driven, hair follicle stem cell activation. Development *135*, 1059–1068.

Osorio, K.M., Lilja, K.C., and Tumbar, T. (2011). Runx1 modulates adult hair follicle stem cell emergence and maintenance from distinct embryonic skin compartments. J. Cell Biol. *193*, 235–250.

Porrello, E.R., Mahmoud, A.I., Simpson, E., Hill, J.A., Richardson, J.A., Olson, E.N., and Sadek, H.A. (2011). Transient regenerative potential of the neonatal mouse heart. Science *331*, 1078–1080.

Pournasr, B., Khaloughi, K., Salekdeh, G.H., Totonchi, M., Shahbazi, E., and Baharvand, H. (2011). Concise review: alchemy of biology: generating desired cell types from abundant and accessible cells. Stem Cells *29*, 1933–1941.

Rompolas, P., Mesa, K.R., and Greco, V. (2013). Spatial organization within a niche as a determinant of stem-cell fate. Nature *502*, 513–518.

Samokhvalov, I.M., Samokhvalova, N.I., and Nishikawa, S. (2007). Cell tracing shows the contribution of the yolk sac to adult haematopoiesis. Nature *446*, 1056–1061.

Scheitz, C.J., Lee, T.S., McDermitt, D.J., and Tumbar, T. (2012). Defining a tissue stem cell-driven Runx1/Stat3 signalling axis in epithelial cancer. EMBO J. *31*, 4124–4139.

Schwitalla, S., Fingerle, A.A., Cammareri, P., Nebelsiek, T., Göktuna, S.I., Ziegler, P.K., Canli, O., Heijmans, J., Huels, D.J., Moreaux, G., et al. (2013). Intestinal tumorigenesis initiated by dedifferentiation and acquisition of stem-cell-like properties. Cell *152*, 25–38.

Simons, B.D., and Clevers, H. (2011). Strategies for homeostatic stem cell self-renewal in adult tissues. Cell *145*, 851–862.

Spradling, A., Fuller, M.T., Braun, R.E., and Yoshida, S. (2011). Germline stem cells. Cold Spring Harb. Perspect. Biol. *3*, a002642.

Tumbar, T., Guasch, G., Greco, V., Blanpain, C., Lowry, W.E., Rendl, M., and Fuchs, E. (2004). Defining the epithelial stem cell niche in skin. Science *303*, 359–363.

Waddington, C.H. (1957). The Strategy of the Gene (London: George Allen and Unwin).

Yanger, K., Zong, Y., Maggs, L.R., Shapira, S.N., Maddipati, R., Aiello, N.M., Thung, S.N., Wells, R.G., Greenbaum, L.E., and Stanger, B.Z. (2013). Robust cellular reprogramming occurs spontaneously during liver regeneration. Genes Dev. *27*, 719–724.

Zhang, Y.V., Cheong, J., Ciapurin, N., McDermitt, D.J., and Tumbar, T. (2009). Distinct self-renewal and differentiation phases in the niche of infrequently dividing hair follicle stem cells. Cell Stem Cell *5*, 267–278.

Zhang, Y.V., White, B.S., Shalloway, D.I., and Tumbar, T. (2010). Stem cell dynamics in mouse hair follicles: a story from cell division counting and single cell lineage tracing. Cell Cycle *9*, 1504–1510.